eNeuro

Research Article: New Research | Sensory and Motor Systems

Aging but not age-related hearing loss dominates the decrease of parvalbumin immunoreactivity in the primary auditory cortex of mice

https://doi.org/10.1523/ENEURO.0511-19.2020

Cite as: eNeuro 2020; 10.1523/ENEURO.0511-19.2020

Received: 8 December 2019
Revised: 6 March 2020
Accepted: 22 March 2020

Aging but not age-related hearing loss dominates the decrease of parvalbumin immunoreactivity in the primary auditory cortex of mice

Abbreviated title: Reduced PV immunoreactivity in the aged mouse pAC

Authors:

Meike M Rogalla, MSc (corresponding author)
Department for Neuroscience
Carl von Ossietzky University Oldenburg
Cluster of Excellence Hearing4all
26111 Oldenburg, Germany
Tel: +49 441 798 3782
meike.rogalla@uni-oldenburg.de

Dr. K Jannis Hildebrandt
Department for Neuroscience
Carl von Ossietzky University Oldenburg
Cluster of Excellence Hearing4all
26111 Oldenburg, Germany
Tel: +49 441 798 3383
jannis.hildebrandt@uni-oldenburg.de

Pages:	23
Figures:	4+1
Tables:	2
Words in Abstract:	215
Introduction:	431
Discussion:	1647

Author Contribution: Conceptualization: M.M.R. and K.J.H., Methodology: M.M.R. and K.J.H., Investigation: M.M.R., Analysis: M.M.R. and K.J.H. Writing: M.M.R, Funding Acquisition, K.J.H.; Resources, K.J.H., Supervision, M.M.R. and K.J.H.

Conflict of interest: Authors declare there are no competing financial interests

Funding sources: This work was supported by the DFG Cluster of Excellence "Hearing4all" [grant number EXC 1077/1].

Acknowledgements: The authors thank L Ebbers and ML Kessler for their helpful comments and productive scientific discussions. Additionally, the authors thank A Sommer and Y Kleinhans for the support with immunostaining and L Osterhagen for the support with ABR recordings.

Animal welfare authorities /Regulations: Lower Saxony State Office for Consumer Protection and Food Safety / LAVES, permission number 33.9-43502-04-13/1271

Aging but not age-related hearing loss dominates the decrease of parvalbumin immunoreactivity in the primary auditory cortex of mice

Abstract

Alterations in inhibitory circuits of the primary auditory cortex (pAC) have been shown to be an aspect of aging and age-related hearing loss (AHL). Several studies reported a decline in parvalbumin (PV) immunoreactivity in aged rodent pAC of animals displaying AHL and conclude a relationship between reduced sensitivity and declined PV immunoreactivity. However, it remains elusive whether AHL or a general molecular aging is causative for decreased PV immunoreactivity. In this study, we aimed to disentangle the effects of AHL and general aging on PV immunoreactivity patterns in inhibitory interneurons of mouse pAC. We compared young and old animals of a mouse line with AHL (C57BL/6) and a mutant (C57B6.CAST-*Cdh23*$^{Ahl+}$) that is not vulnerable to AHL according to their hearing status by measuring auditory brainstem responses (ABR) and by an immunohistochemical evaluation of the PV immunoreactivity patterns in two dimensions (rostro-caudal and layer) in the pAC. Although AHL could be confirmed by ABR measurements for the C57BL/6 mice, both aged strains showed a similar reduction of PV^{+} positive interneurons in both, number and density. The pattern of reduction across the rostro-caudal axis and across cortical layers was similar for both aged lines. Our results demonstrate that a reduced PV immunoreactivity is a sign of general, molecular aging and not related to age related hearing loss.

Significance Statement

Deficiency of sensory functions is one of the major detriments of aging. In hearing, aging affects both the periphery and inhibitory circuits in the central system, resulting in hearing loss and altered perception. Centrally, the major subclass of inhibitory interneurons (parvalbumin positive) shows reduced parvalbumin immunoreactivity, which is believed to be related to altered inhibition. Identifying the factor that dominates this decline is important to understand molecular aging in the central auditory system. Here, we demonstrate that the decreased parvalbumin immunoreactivity in the primary auditory cortex of mice is dominated by general aging rather than age-related hearing loss, suggesting that altered cortical inhibition in the auditory system may not be secondary to peripheral changes, but a consequence of aging per se.

Introduction

Age-related hearing loss (AHL), also referred to as presbycusis, is one of the most common sensory impairments worldwide, approximately affecting one third of adults above 65 years in forms of progressive loss of auditory function (Loughrey et al., 2018; Roth et al., 2011).

On the physiological level, the loss of hearing during aging is usually related to a loss of sensory hair cells or a decline of spiral ganglion cells (Frisina et al., 2016). Such age-related morphological changes have not only been observed in humans, but also in laboratory rodents, especially in mice (Hequembourg and Liberman, 2001; Li et al., 2002; McFadden et al., 2001) which therefore have been suggested to be a suitable model of AHL (Bowl and Dawson, 2014; Gratton and Vázquez, 2003).

The decline of peripheral signal transmission has been linked to subsequent pathological changes within the central nervous system, especially in the primary auditory cortex, pAC (Eckert et al., 2012). Especially alterations in inhibitory circuits of the pAC have been linked to hearing loss and the aged auditory system (Kotak, 2005; Peelle and Wingfield, 2016; Takesian et al., 2012). The largest class of cortical GABAergic interneurons, the parvalbumin (PV) neurons, are believed to play an important role when it comes to loss-of-input dependent changes in the neuronal inhibitory circuits of pAC. Several studies reported a relationship between AHL and a decline in PV immunoreactivity in the rodent auditory cortex (Brewton et al., 2016; de Villers-Sidani et al., 2010; Martin del Campo et al., 2012) whereas others report a decline in PV immunoreactivity for several cortical areas, unrelated to any decline in sensory function (Miettinen et al., 1993; Ueno et al., 2018). Due to these contrary findings, it remains elusive whether a decline of PV immunoreactivity in pAC is a result of progressive AHL and the loss of input or if it is just a general phenomenon in the aging central (auditory) system.

In this study, we aimed to resolve the effect of aging and AHL on the PV immunoreactivity in the primary auditory cortex of mice. To this end, we used a mouse line with a rapid, progressive development of AHL (C57BL/6) and the mutant C57B6.CAST-*Cdh23*$^{Ahl+}$, a congenic strain that carries the wildtype allele of *Cdh23,* producing C57BL/6 mice that are not vulnerable to AHL (Johnson et al., 1997; Keithley et al., 2004; Mock et al., 2016). We compared young and old animals of both lines according to their hearing status by using auditory brainstem response measurements and an immunohistochemical evaluation of the PV immunoreactivity patterns in two dimensions (rostro-caudal and layer) of the primary auditory cortex.

Methods

Experimental Groups

All animal experiments were performed in accordance with the animal welfare regulations of Lower Saxony and with the approval from the local authorities (State Office for Consumer Protection and Food Safety / LAVES, permission number 33.9-43502-04- 13/1271).

In total, 43 mice were used in this study, of which 21 were used for ABR measurements only, 15 in histology only and 7 animals in both.

Male C57BL/6J (stock number 017320; RRID: JAX:017320) mice were used in this study to serve as an animal model with age-related hearing loss. In contrast, male C57B6.CAST-*Cdh23*$^{Ahl+}$ (stock number 002756; RRID: JAX:002756) mice were used as an animal model without the development of AHL. Both strains were in-bred animals, originating from purchased breeding pairs (Jackson Laboratory, USA) and kept in small colonies with *ad libitum* access to water and food in the local animal facility under standardized conditions until terminal experiments.

The age groups were designed as follows: young animals (10-12 weeks) of both strains (young^{B6}, n = 11) and young$^{B6.CAST}$, n = 7) and aged animals (12-15 month) with age-related hearing loss (aged^{B6}, n = 13) and without (aged$^{B6.CAST}$, n = 12, for details, see table 1).

Evaluation of Hearing Status – Auditory Brainstem Response (ABR)

Animals were anesthetized with Ketamine (initial 10 mg/kg, maintenance 2.5 mg/kg) and Medetomidine (initial 0.083 mg/kg, maintenance 0.01mg/kg). The state of anesthesia was checked in regular intervals, if needed anesthesia was toped up with the maintenance dose

(typically every 1.5 hours). Needle electrodes were placed subcutaneous with the recording electrode at the neck and the reference electrode at the vertex. The electrode signal was bandpass filtered (300 Hz–30 kHz) and amplified by an ISO-80 Bio-amplifier (World Precision Instruments, Sarasota, FL), before A/D-converted through a Fireface UC 24-bit sound device at a sample rate of 96 kHz. The same device was used for stimulus delivery. Stimuli were created by a custom MATLAB application. The sound was binaurally delivered directly into the ear canal of the animal through horns that were attached to Vifa/Peerless XT-300 K4 loudspeakers. The system was calibrated prior to recording using small microphones (Knowles FG-23329, Itasca, IL) that were inserted into replicas of mice ear canals.

In order to determine hearing thresholds at different tone frequencies, tone pips (10 ms, 2 ms cosine ramps at on- and offset) were presented binaurally at 4, 8, 12, 16, 20, 24 and 30 kHz. The intensity was varied between 35 and 95 dB SPL in steps of 5 dB. Inter-stimulus intervals were randomly chosen from the interval 50 - 150 ms. The sequence of stimuli was random. An automatic online artifact rejection algorithm discarded trials with muscle potential artifacts according to a pre-set threshold. ABR data was recorded continuously and saved for offline evaluation.

Histology

Animals were injected with a lethal overdose of pentobarbital (Narcoren, Boehringer Ingelheim, Germany) and transcardially perfused with phosphate buffer (PB, pH = 7.4) followed by fixative (4% paraformaldehyde in PB). The brains were removed and kept in immersion fixative overnight at 4 °C, followed by 4 rinsing steps the next day (PB). For cryoprotection, brains were stored in 30 % sucrose solution in PB for 2-3 days at 4 °C. After complete saturation, brains were frozen using tissue freezing medium (TFM-5, TBS) and stored at -20 °C.

Coronal frozen slices (25 µm) containing pAC were cut (CM 1950, Leica, Germany) in series of 4. A mark was placed subcortically into the right hemisphere using a cannula for post-staining distinctness. Slices of the first series were directly mounted on gelatin-coated object slides and air-dried for Nissl staining. Remaining slices of series 2-4 were stored in a 24-well plate/series, containing cryoprotection solution (30 % ethylenglycol and 30 % sucrose in PBS) and stored at -20°C until immunohistochemistry.

Nissl Staining

The total number of cortical neurons may decrease during aging and this effect may be stronger in animals suffering from hearing loss. To account for this, an evaluation of the total number of neurons in the pAC, a standard Nissl protocol using 0.1 % cresyl violet in watery solution was applied. After staining, object slides were rinsed in distilled water, followed by differentiation and complete dehydration with ascending alcohol concentrations. After clearing with xylol, object slides were cover slipped using rapid non-aqueous mounting medium (Entellan, 107960, Merck, Germany).

Parvalbumin Immunohistochemistry

The slices for visualization of PV^+ interneurons were treated free floating. Slices of one series were rinsed 5 x 5 minutes in phosphate buffered saline (PBS, pH = 7.4), followed by 10 minutes permeabilization in 0.5 % Triton X-100 in PBS at room temperature. To prevent nonspecific binding, epitopes on the tissue were blocked with 10 % normal goat serum in PBS for 1.5 hours at room temperature, followed by 24 hours incubation with a polyclonal primary antibody against PV produced in rabbit (1:800, rabbit anti-parvalbumin PV27, Swant Swiss Antibodies, Switzerland RRID:AB_2631173) diluted in blocking solution at 4 °C. After rinsing in PBS for 5

x 5 minutes, slices were incubated with the polyclonal secondary antibody produced in goat (1:200, goat anti-rabbit Alexa Flour 488, ab150077, abcam, USA) in blocking solution for 5 hours at room temperature in darkness. Slices were rinsed 3 x 5 minutes in PBS and mounted on object slides (Superfrost Plus, Thermo Scientific, USA) and cover slipped with anti-fade mounting medium (Vectashield H-1000, Vector Laboratories, USA).

Data Analysis and Statistics

Auditory Brainstem Response (ABR)

For every stimulus at least 400 artifact free trials were recorded. Thresholds at individual frequencies were determined by eye from the average stimulus-aligned traces at each frequency as the lowest level that evoked an auditory brainstem-response (Fig. 2A). If no response could be evoked up to 95 dB, threshold was set to 95 dB, which was the highest level we were able to present without distortions.

Histology

For quantitative analysis of the PV immunoreactivity in young and old animals (with and without AHL), pAC was photographed at 10 x magnification using an Axioskop 2 MOT Plus (Carl Zeiss Microscopy GmbH, Germany) equipped with a camera (Eos 7D, Canon, Japan). The pAC was identified by using anatomical landmarks as reference, a method adopted from (Martin del Campo et al., 2012) and a mouse brain atlas as reference (Allen Mouse Brain volumetric atlas 2012, https://mouse.brain-map.org). Images were acquired directly above the center by placing the pAC into the middle of the camera section (see fig. 1 A). Images were exported as TIFF. Neurons and PV^+ neurons were counted within the region of interest (ROI, 400 µm height for PV slices and 50 µm for Nissl slices, see fig. 1 B & C) which was placed above the center. We

previously confirmed the position of auditory cortex in B6.CASTanimals (extended data, figure 2-1 and Gothner et al., 2019). Counting was performed manually by a person who was blind to the experimental condition using the cell counter plugin in Fiji for non-automated quantification (Schindelin et al., 2012). Only neurons with a clearly identifiable soma were labeled as positive. In Nissl slices, only cells with the neuron-characteristics perikarya and soma staining were counted (see figure 2C). Neurons which were touching the lateral (relative to cortex) border where included, whereas those touching the medial border of the ROI were excluded.

For each animal, at least eight slices (both hemispheres), distributed along the rostro caudal axis were analyzed to calculate the mean number of PV^+ neurons. The depth of the cortex (from pia to white matter) was labeled in each slice to calculate the mean density of PV^+ neurons (neurons/mm^2). The total number of neurons (Nissl) was multiplied by the factor of eight and the mean served as a control for the evaluation of possible cell loss during aging and/or AHL.

All variables (number of neurons, number of PV^+ neurons and density of PV^+ neurons) were statistically analyzed (IBM SPSS Statistics vers. 25, IBM, USA) for the following groups: young (including both, $young^{B6}$ and $young^{B6.CAST}$), $aged^{B6}$ and $aged^{B6.CAST}$. Data were tested for normal distribution and homogeneity of variances prior to the analysis of variance (ANOVA). Effect size was calculated as $= \sqrt{\eta^2/1-\eta^2}$. Power (1-β) was calculated using G*Power (Faul et al., 2007). A one-sided post-hoc test (Dunnett) was applied according to the hypothesis of a reduction in PV cells in aged animals of both groups ($young^{B6/B6.CAST} > aged^{B6}$ and $aged^{B6.CAST}$). Due to the small sample size of all groups, the level of significance was set to $\alpha = 0.01$.

Differences in number and density of PV^+ interneurons might not be observable in the whole sample but could be dependent of the cell position in the dimension of layer or rostro-caudal axis. In order to evaluate the laminar distribution of PV^+ in the different animal groups, cell

158 coordinates were projected onto the axis between pia and white-matter boarder in each individual
159 slice. Laminar position was calculated as the distance from the pia relative to pia-white matter
160 distance. Laminar position was binned in 10 equally sized windows and averaged to obtain a
161 laminar distribution for each animal. Subsequently, mean distributions for each group were
162 calculated.
163 In order to obtain a position along the rostro-caudal axis, slices were aligned to the Allen Mouse
164 Brain volumetric atlas (Allen Mouse Brain volumetric atlas 2012, https://mouse.brain-map.org)
165 and referenced to bregma coordinates. Slice positions were binned in 204 µm windows ranging
166 from 2458 to 3681 µm caudal relative to bregma. All cells within a specific laminar bin and on
167 slices within each rostro-caudal bin were counted to obtain distributions of PV^+ neurons along
168 the rostral-caudal and laminar axes for each animal group.

Results

Aged animals from the B6.CAST line do not show AHL

169 We aimed to test whether the previously reported decline in PV immunoreactivity in the auditory
170 cortex of C57/B6 mice could be a result of their early onset age related hearing loss (AHL). To
171 this end we compared aged wild type C57/B6 mice ($aged^{B6}$) with a control group of the mutant
172 C57B6.CAST-$Cdh23^{Ahl+}$ ($aged^{B6.CAST}$) that is not susceptible to AHL.
173 In a first step, we therefore confirmed the difference in AHL between the two aged groups (fig.
174 2). In $aged^{B6}$ we found an increase of the threshold over the entire tested frequency range (fig.
175 2B) with the mean threshold increasing from 44.6 ± 7.2 dB SPL (mean ± standard deviation, n =
176 6) to 89.8 ± 3.2 dB SPL (n = 7). For the B6.CAST group, we could observe almost no change in
177 thresholds across all frequencies (mean thresholds young 44.0 ± 7.0 dB SPL, n = 6 vs. 47.2 ± 8.3

dB SPL in the aged$^{B6.CAST}$ group, n = 9). ABR thresholds for young animals of the two lines were not different (44.6 ± 7.2 dB SPL vs. 44.0 ± 7.0 dB SPL). Consequently, data from young^{B6} and young$^{B6.CAST}$ have been pooled in the immunohistochemical experiments.

Aging causes a reduction in PV immunoreactivity in the pAC of mice with and without AHL

In the present study, we investigated the number and density of PV^{+} neurons in the primary auditory cortex of young$^{B6/B6.CAST}$ (both lines pooled) and old mice with and without the presence of AHL, previously determined by the ABR measurements.

Possibly, a decline in total number of neurons may be stronger in one of the aged groups which could confound the interpretation of the total number of PV+ cells. To ensure that our results of the immunohistochemical verification were not influenced by a global decline in cortical neurons, the total number of neurons was investigated using a Nissl protocol. A mild, non-significant decrease of neurons was present in aged$^{B6.CAST}$ and aged^{B6} compared to young$^{B6/B6.CAST}$ (fig. 3 A, $F(2; 19) = 3.523$; $p = 0.05$, ANOVA; $f = 0.61$, $1\text{-}\beta = 0.374$; post-hoc pair-wise comparison Dunnett, one-sided, young$^{B6/B6.CAST}$ > aged^{B6}: $p = 0.021$; young$^{B6/B6.CAST}$ > aged$^{B6.CAST}$: $p = 0.056$).

The immunohistochemical verification has been performed to investigate whether a) a decline of PV immunoreactivity exists during aging and b) if it is stronger in animals suffering from progressive AHL. A significant decrease in number of PV^{+} neurons could be observed for aged$^{B6.CAST}$ and aged^{B6} groups (fig 3 B, $F(2; 19)\ 2 = 1.182$; $p < 0.001$, ANOVA ; $f = 1.49$, $1\text{-}\beta = 0.9993$). The one-sided pairwise comparison to young$^{B6/B6.CAST}$ animals revealed a strong difference for both, young$^{B6/B6.CAST}$ vs. aged^{B6} and young$^{B6/B6.CAST}$ vs. aged$^{B6.CAST}$ ($p < 0.001$).

198 Additionally, we investigated the density of PV^+ neurons by taking the cortical depth of each
199 analyzed imaged into account (400 µm ROI width x cortical depth, calculated as neurons/mm^2,
200 fig. 3 C). The density of PV^+ neurons/mm^2 differed significantly (ANOVA, $F(2; 19) = 9.301$; $p <$
201 0.01; $f = 0.99$, $1\text{-}\beta = 0.884$). Similar to the absolute counts, we found a significant lower density
202 in both $aged^{B6}$ vs. $young^{B6/B6.CAST}$ ($p < 0.01$) and $aged^{B6.CAST}$ vs. $young^{B6/B6.CAST}$ ($p = 0.001$).
203 Differences in number and density of PV^+ interneurons might not be observable in the whole
204 sample but could be dependent of the cell position in two dimensions: layer positions defined as
205 cortical depth and along the rostro-caudal axis. In order to receive a detailed description of the
206 immunoreactivity pattern, we performed an analysis of PV immunoreactivity in in these two
207 dimensions in the primary auditory cortex of all animals. We observed a clear layer dependence
208 of PV^+ neurons revealed by the analysis of the density as a factor of cortical depth, with a strong
209 peak in deep (subgranular) layers (fig. 4 A). The largest density was present in the middle layers
210 of pAC (maximum just below layer IV). This layer dependence occurred with a nearly uniform
211 distribution across the rostra-caudal axis of pAC (data of all animals, fig. 4 B). Subsequently, we
212 analyzed layer dependence and rostro-caudal distribution for the factor of age and AHL. We
213 could not observe a robust overall pattern of reduction along the rostro-caudal axis, but slightly
214 higher reduction of PV^+ neurons in the rostral portion of pAC in $aged^{B6}$ compared to young and
215 $aged^{B6.CAST}$ (fig. 4 C). In contrast, the reduction was stronger in the caudal region in aged animals
216 without AHL ($aged^{B6.CAST}$). When comparing groups according to the factor of cortical depth
217 (fig. 4 D), the reduction across lamina was uniform in both, $aged^{B6.CAST}$ and $aged^{B6}$. PV density in
218 the middle layers was mildly more reduced for animals from the $aged^{B6.CAST}$, group than from
219 $aged^{B6}$. In summary, the combined pattern of reduction (fig. 4 E) across laminar and rostro-

caudal axis appears to be very similar for aged animals with AHL (aged^{B6}) and without (aged$^{B6.CAST}$).

Discussion

We aimed to reveal whether a decrease in PV immunoreactivity during aging is stronger in the presence of AHL, as previously indicated (Brewton et al., 2016; de Villers-Sidani et al., 2010; Martin del Campo et al., 2012). On that account, we investigated the hearing thresholds and the PV immunoreactivity in the pAC of aged animals from a mouse line with progressive, early onset AHL (C57BL/6J) and from a congenic strain which is not vulnerable to AHL (C57B6.CAST-Cdh23^{Ahl+}), in comparison with young animals. The main outcome of this study is a decline in PV immunoreactivity in the primary auditory cortex of aged mice, regardless of AHL. Although AHL could be confirmed by our ABR measurements for the aged^{B6} animals (fig. 2), both aged strains showed a similar reduction of PV$^+$ positive interneurons in pAC in both number and density (fig. 3). The pattern of reduction across the rostro-caudal axis and across cortical layers was similar in both strains (fig. 4).

Specificity of reduction of PV cells

We investigated PV immunoreactivity in the pAC of all experimental groups by an indirect, immunofluorescent approach, using a primary antibody against PV. Additionally, as a control, the total number of neurons was evaluated to test for possible unequal cell loss between aged groups, following a standard Nissl protocol. Reduced PV immunoreactivity and thus a smaller number of positive cells may have been the results of a global loss of neurons for the aged groups compared to young animals and may be more severe in animals suffering from AHL. In

239 our study, we found the total number of neurons in the pAC to be decreased in both aged groups,
240 albeit not significantly. This mild, non-significant decrease in number of neurons for aged
241 animals has been previously reported, at least for the rat auditory cortex (Burianová et al., 2015).
242 In relation to our data from the evaluation of PV immunoreactivity (fig. 3B/C), it can be
243 concluded that a decreased number of PV^+ is not solely based on a cortical neuronal decline in
244 only one of the experimental groups. However, the identity of the lost neurons (reflected by the
245 mild decrease in number of neurons) cannot be clearly defined with our experimental approach.
246 It remains to be shown whether PV^+ neurons remain intact but display a reduced protein
247 expression or if the density of these specific inhibitory interneurons is decreased.

248 Reduction of PV^+ interneurons is present in aged animals with preserved hearing thresholds

249 Regarding the number and density of PV^+ neurons, aged$^{B6.CAST}$ and aged^{B6} show a decrease of
250 both. Indeed, a reduction in PV immunoreactivity seems to be dominated by the factor age rather
251 than by hearing loss. This is in line with results from other studies, reporting decreased inhibitory
252 properties in the aged auditory cortex independent of hearing status (Kessler et al., 2019; Ueno et
253 al., 2018) and a reduction in PV^+ neurons in other cortical areas, like somatosensory or motor
254 (Miettinen et al., 1993).
255 One main reason for controversial results might be strong strain differences of PV
256 immunoreactivity levels in animals. These differences are not only present on the molecular but
257 also on the physiological level (Bowen et al., 2019; Brewton et al., 2016). All work that has been
258 done so far to reveal the influence of AHL on the PV immunoreactivity pattern used either two
259 different strains of laboratory rodents with/without the development of AHL (Brewton et al.,
260 2016; Ouda et al., 2008) or compared old vs. young animals of the same strain (de Villers-Sidani
261 et al., 2010; Martin del Campo et al., 2012). It is possible that not only physiological properties

differ between strains, but also the development of PV immunoreactivity patterns over time. In our study, the only difference between the two mouse strains used is the wildtype allele of *Cdh23* in aged$^{B6.CAST}$ animals, eliminating the possibility of general strain differences in basal PV immunoreactivity patterns. However, it cannot be ruled out that patterns of PV immunoreactivity in the central auditory system depend on the genetic, peripherally acting cause of age related hearing loss. As the cause in our hearing impaired aged^{B6} animals, the missense mutation of *Cdh23* is believed to result in a defective encoded protein that acts as a component of the stereocilia tip links in hair cells. The defect can cause a weakening of the tip links over time, which may result in progressively impaired mechanotransduction in the aging individual (Johnson et al., 2010; Kazmierczak et al., 2007; Schwander et al., 2009). Whether our results can be directly transferred to other mutations needs to be further investigated, e.g. in mutations of *Sod1,* which encodes for a defective superoxide dismutase, resulting in increased oxidative stress and therewith hair cell loss in the inner ear (Jiang et al., 2007; Johnson et al., 2010; McFadden et al., 2001). However, our results can be interpreted as a first step towards a better understanding about the central molecular alterations in Cdh23-mediated presbycusis.

Pattern of PV immunoreactivity along the rostro-caudal axis and cortical depth

To get an overall impression of the neuronal PV pattern in the primary auditory cortex of young, aged and aged mice expressing hearing loss, we provide a 2-dimensional descriptive analysis of the rostro-caudal and layer-dependent distribution of PV^+ interneurons. Our data indicate an overall similar rostro-caudal distribution for all tested groups. However, the loss of PV immunoreactivity varies considerably between adjacent individual rostro-caudal sections (fig. 4 C) and may show differences between the groups. For a more fine-grained, unbiased evaluation of differences between immunoreactivity patterns, it should be considered to analyze multiple

284 samples per animal along the rostro-caudal axis of the structure of interest as done in this study.
285 Small sample sizes confined to narrow rostro-caudal sections could lead to false-positive
286 differences that might disappear when analyzing a sample size distributed along the rostro-caudal
287 axis or vice versa.
288 The PV density as a function of cortical depth peaks in middle layers, with a small population of
289 neurons in the deeper and the fewest number in the superficial layers (fig. 4 D) as previously
290 revealed by others (Brewton et al., 2016; del Rio et al., 1994; Martin del Campo et al., 2012;
291 Ueno et al., 2018). Regarding age and hearing status, we could not detect a difference between
292 distributions of an aged$^{B6.CAST}$ or an aged^{B6} animal. Thus, an altered density of PV^+ neurons along
293 the cortical depth is related to the factor age and remains unaltered by hearing status, similar to
294 what we observed for PV immunoreactivity along the rostro-caudal axis.

Reduced PV immunoreactivity in the primary auditory cortex - a sign of central molecular aging in the mouse model

295 The C57BL/6 mouse is commonly used as an animal model to study presbycusis due to its
296 progressive, early onset AHL which is the result of the degenerating basal portion of the cochlear
297 (Ison et al., 2007; Martin del Campo et al., 2012; Park et al., 2010). This process can be
298 confirmed by analyzing auditory brainstem responses and it has been shown to become
299 histologically detectable by the age of three month (Park et al., 2010). In parallel, a second
300 aging-induced process seem to act on the central (auditory) system in form of reduced PV
301 immunoreactivity in the inhibitory network of the cortex. Our data indicates that this process is
302 independent of declined hearing sensitivity and should rather be interpreted as a sign of central
303 molecular aging. The consequences of reduced intraneuronal protein levels in inhibitory system
304 are not fully understood yet. Hence, it remains controversial to what extent a reduction of PV

immunoreactivity affects inhibition and therewith central sensory processing in the (auditory) cortex.

Parvalbumin itself as a calcium-binding protein is believed to serve the distinct function of buffering intracellular Ca^{2+}, enabling the neuron to fire rapid spike trains and protecting it from toxic intracellular calcium levels (Fairless et al., 2019; Ferguson and Gao, 2018). This might support the unique function of this neuronal subtype: parvalbumin positive interneurons are known for their remarkable fast spiking phenotype with a local widespread of activity regulating contacts to nearly every pyramidal neuron in their surrounding (Ferguson and Gao, 2018; Kawaguchi, 1997; Packer and Yuste, 2011). On a functional level, this organization principle allows for strong feedback and feedforward inhibition with a precision in the millisecond range (Cardin, 2018; Hu et al., 2014). A change in the physiology of PV^+ cells may be particularly impactful in the auditory cortex, where precise modulation of sensory input is of great importance as it sharpens spike timing, shapes receptive fields, provides gain control and is involved in the generation of network oscillations (Gothner et al., 2019; Hu et al., 2014; Moore and Wehr, 2013; Sohal et al., 2009; Wehr and Zador, 2003). In that context, a reduced PV immunoreactivity could result in declined inhibitory properties in cortical circuits, which seems to be independent of AHL.

An additional potential role of PV that is discussed in current research is its involvement in (synaptic) plasticity: PV seems to prevent cumulative facilitation and maintains the strength of the synapse near its resting level (Caillard et al., 2000; Tripodi et al., 2018). Additionally, a few studies indicate that the PV immunoreactivity pattern cannot be interpreted as a static rather than an ongoing plastic process, influenced by environmental factors as previously demonstrated by

de Villers-Sidani and colleagues (2010), who showed that decreased PV immunoreactivity in the aged auditory cortex of rats can be recovered by auditory training.

Given the importance of PV^+ inhibition and the strong reduction of PV immunoreactivity in the aging auditory cortex as shown here, further research is urgently needed to reveal the actual consequences of age-related reduction of PV immunoreactivity on inhibitory circuits on a physiological level. However, given the results presented here, physiological and possibly perceptual consequences of PV^+ reduction in pAC will have to be seen as a result of general, molecular aging in the auditory cortex instead of being restricted to individuals suffering from AHL.

References

Bowen Z, Winkowski DE, Kanold PO (2019) Functional Organization of Mouse Primary Auditory Cortex in adult C57BL/6 and F1 (CBAxC57) mice. bioRxiv.

Bowl MR, Dawson SJ (2014) The Mouse as a Model for Age-Related Hearing Loss - A Mini-Review. Gerontology 61:149–157.

Brewton DH, Kokash J, Jimenez O, Pena ER, Razak KA (2016) Age-Related Deterioration of Perineuronal Nets in the Primary Auditory Cortex of Mice. Frontiers in Aging Neuroscience 8.

BurianovÃ¡ J, Ouda L, Syka J (2015) The influence of aging on the number of neurons and levels of non-phosporylated neurofilament proteins in the central auditory system of rats. Frontiers in Aging Neuroscience 7.

Caillard O, Moreno H, Schwaller B, Llano I, Celio MR, Marty A (2000) Role of the calcium-binding protein parvalbumin in short-term synaptic plasticity. Proceedings of the National Academy of Sciences 97:13372–13377.

Cardin JA (2018) Inhibitory Interneurons Regulate Temporal Precision and Correlations in Cortical Circuits. Trends in Neurosciences 41:689–700.

de Villers-Sidani E, Alzghoul L, Zhou X, Simpson KL, Lin RCS, Merzenich MM (2010) Recovery of functional and structural age-related changes in the rat primary auditory cortex with operant training. Proceedings of the National Academy of Sciences 107:13900–13905.

del Rio J, de Lecea L, Ferrer I, Soriano E (1994) The development of parvalbumin-immunoreactivity in the neocortex of the mouse. Developmental Brain Research 81:247–259.

Eckert MA, Cute SL, Vaden KI, Kuchinsky SE, Dubno JR (2012) Auditory Cortex Signs of Age-Related Hearing Loss. Journal of the Association for Research in Otolaryngology 13:703–713.

Fairless R, Williams SK, Diem R (2019) Calcium-Binding Proteins as Determinants of Central Nervous System Neuronal Vulnerability to Disease. International Journal of Molecular Sciences 20:2146.

Faul F, Erdfelder E, Lang A-G, Buchner A (2007) G*Power 3: A flexible statistical power analysis program for the social, behavioral, and biomedical sciences. Behavior Research Methods 39:175–191.

Ferguson BR, Gao W-J (2018) PV Interneurons: Critical Regulators of E/I Balance for Prefrontal Cortex-Dependent Behavior and Psychiatric Disorders. Frontiers in Neural Circuits 12.

Frisina R, Ding B, Zhu X, Walton J (2016) Age-related hearing loss: prevention of threshold declines, cell loss and apoptosis in spiral ganglion neurons. Aging 8:2081–2099.

Gothner T, Gonçalves PJ, Sahani M, Linden JF, Hildebrandt KJ (2019) Sustained Activation of PV+ Interneurons in Auditory Cortex Enables Robust Divisive Gain Control for Complex and Naturalistic Stimuli (preprint). Neuroscience.

Gratton MA, Vázquez AE (2003) Age-related hearing loss: current research. Curr Opin Otolaryngol Head Neck Surg 11:367–371.

Hequembourg S, Liberman MC (2001) Spiral Ligament Pathology: A Major Aspect of Age-Related Cochlear Degeneration in C57BL/6 Mice. Journal of the Association for Research in Otolaryngology 2:118–129.

379 Hu H, Gan J, Jonas P (2014) Fast-spiking, parvalbumin+ GABAergic interneurons: From
380 cellular design to microcircuit function. Science 345.
381 Ison JR, Allen PD, O'Neill WE (2007) Age-Related Hearing Loss in C57BL/6J Mice has both
382 Frequency-Specific and Non-Frequency-Specific Components that Produce a
383 Hyperacusis-Like Exaggeration of the Acoustic Startle Reflex. Journal of the Association
384 for Research in Otolaryngology 8:539–550.
385 Jiang H, Talaska AE, Schacht J, Sha S-H (2007) Oxidative imbalance in the aging inner ear.
386 Neurobiology of Aging 28:1605–1612.
387 Johnson KR, Erway LC, Cook SA, Willott JF, Zheng QY (1997) A major gene affecting age-
388 related hearing loss in C57BL/6J mice. Hearing Research 114:83–92.
389 Johnson KR, Yu H, Ding D, Jiang H, Gagnon LH, Salvi RJ (2010) Separate and combined
390 effects of Sod1 and Cdh23 mutations on age-related hearing loss and cochlear pathology
391 in C57BL/6J mice. Hearing Research 268:85–92.
392 Kawaguchi Y (1997) GABAergic cell subtypes and their synaptic connections in rat frontal
393 cortex. Cerebral Cortex 7:476–486.
394 Kazmierczak P, Sakaguchi H, Tokita J, Wilson-Kubalek EM, Milligan RA, Müller U, Kachar B
395 (2007) Cadherin 23 and protocadherin 15 interact to form tip-link filaments in sensory
396 hair cells. Nature 449:87–91.
397 Keithley EM, Canto C, Zheng QY, Fischel-Ghodsian N, Johnson KR (2004) Age-related hearing
398 loss and the ahl locus in mice. Hearing Research 188:21–28.
399 Kessler M, Mamach M, Beutelmann R, Lukacevic M, Eilert S, Bascuñana P, Fasel A, Bengel
400 FM, Bankstahl JP, Ross TL, Klump GM, Berding G (2019) GABAA Receptors in the
401 Mongolian Gerbil: a PET Study Using [18F]Flumazenil to Determine Receptor Binding
402 in Young and Old Animals. Mol Imaging Biol.
403 Kotak VC (2005) Hearing Loss Raises Excitability in the Auditory Cortex. Journal of
404 Neuroscience 25:3908–3918.
405 Li S, Price SM, Cahill H, Ryugo DK, Shen MM, Xiang M (2002) Hearing loss caused by
406 progressive degeneration of cochlear hair cells in mice deficient for the Barhl1 homeobox
407 gene. Development 129:3523–3532.
408 Loughrey DG, Kelly ME, Kelley GA, Brennan S, Lawlor BA (2018) Association of Age-Related
409 Hearing Loss With Cognitive Function, Cognitive Impairment, and Dementia: A
410 Systematic Review and Meta-analysis. JAMA Otolaryngology–Head & Neck Surgery
411 144:115.
412 Martin del Campo HN, Measor KR, Razak KA (2012) Parvalbumin immunoreactivity in the
413 auditory cortex of a mouse model of presbycusis. Hearing Research 294:31–39.
414 McFadden SL, Ding D, Salvi R (2001) Anatomical, metabolic and genetic aspects of age-related
415 hearing loss in mice. Audiology 40:313–321.
416 Miettinen R, Sirviö J, Riekkinen P, Laakso MP, Riekkinen M, Riekkinen P (1993) Neocortical,
417 hippocampal and septal parvalbumin- and somatostatin-containing neurons in young and
418 aged rats: Correlation with passive avoidance and water maze performance. Neuroscience
419 53:367–378.
420 Mock BE, Vijayakumar S, Pierce J, Jones TA, Jones SM (2016) Differential effects of Cdh23
421 753A on auditory and vestibular functional aging in C57BL/6J mice. Neurobiology of
422 Aging 43:13–22.
423 Moore AK, Wehr M (2013) Parvalbumin-Expressing Inhibitory Interneurons in Auditory Cortex
424 Are Well-Tuned for Frequency. Journal of Neuroscience 33:13713–13723.

425 Ouda L, Druga R, Syka J (2008) Changes in parvalbumin immunoreactivity with aging in the
426 central auditory system of the rat. Experimental Gerontology 43:782–789.
427 Packer AM, Yuste R (2011) Dense, Unspecific Connectivity of Neocortical Parvalbumin-
428 Positive Interneurons: A Canonical Microcircuit for Inhibition? Journal of Neuroscience
429 31:13260–13271.
430 Park S-N, Back S-A, Park K-H, Kim D-K, Park SY, Oh J-H, Park YS, Yeo SW (2010)
431 Comparison of Cochlear Morphology and Apoptosis in Mouse Models of Presbycusis.
432 Clinical and Experimental Otorhinolaryngology 3:126.
433 Peelle JE, Wingfield A (2016) The Neural Consequences of Age-Related Hearing Loss. Trends
434 in Neurosciences 39:486–497.
435 Roth TN, Hanebuth D, Probst R (2011) Prevalence of age-related hearing loss in Europe: a
436 review. European Archives of Oto-Rhino-Laryngology 268:1101–1107.
437 Schindelin J, Arganda-Carreras I, Frise E, Kaynig V, Longair M, Pietzsch T, Preibisch S,
438 Rueden C, Saalfeld S, Schmid B, Tinevez J-Y, White DJ, Hartenstein V, Eliceiri K,
439 Tomancak P, Cardona A (2012) Fiji: an open-source platform for biological-image
440 analysis. Nat Methods 9:676–682.
441 Schwander M, Xiong W, Tokita J, Lelli A, Elledge HM, Kazmierczak P, Sczaniecka A, Kolatkar
442 A, Wiltshire T, Kuhn P, Holt JR, Kachar B, Tarantino L, Muller U (2009) A mouse
443 model for nonsyndromic deafness (DFNB12) links hearing loss to defects in tip links of
444 mechanosensory hair cells. Proceedings of the National Academy of Sciences 106:5252–
445 5257.
446 Sohal VS, Zhang F, Yizhar O, Deisseroth K (2009) Parvalbumin neurons and gamma rhythms
447 enhance cortical circuit performance. Nature 459:698–702.
448 Takesian AE, Kotak VC, Sanes DH (2012) Age-dependent effect of hearing loss on cortical
449 inhibitory synapse function. Journal of Neurophysiology 107:937–947.
450 Tripodi M, Bhandari K, Chowdhury A, Mukherjee A, Caroni P (2018) Parvalbumin Interneuron
451 Plasticity for Consolidation of Reinforced Learning. Cold Spring Harbor Symposia on
452 Quantitative Biology 83:25–35.
453 Tsukano H, Horie M, Hishida R, Takahashi K, Takebayashi H, Shibuki K (2016) Quantitative
454 map of multiple auditory cortical regions with a stereotaxic fine-scale atlas of the mouse
455 brain. Scientific reports 1–13.
456 Ueno H, Takao K, Suemitsu S, Murakami S, Kitamura N, Wani K, Okamoto M, Aoki S, Ishihara
457 T (2018) Age-dependent and region-specific alteration of parvalbumin neurons and
458 perineuronal nets in the mouse cerebral cortex. Neurochemistry International 112:59–70.
459 Wehr M, Zador AM (2003) Balanced inhibition underlies tuning and sharpens spike timing in
460 auditory cortex. Nature 426:442–446.

Figure Legends

Figure 1 – Hearing status of the different groups. A: Examples of averaged ABR traces in response to tone pips at 4 kHz, played back at levels ranging from 40 to 80 dB. The dashed line indicates the onset of a 10 ms tone pip. The asterisks mark the level at which the threshold was set. Left: individual from the agedB6 group, right: animal from the agedB6.CAST group without AHL – both animals were measured at an age of 14 month. B: Mean threshold for all four groups at different sound frequencies. Circles depict B6 animals, squares display animals from the B6.CAST line. Open symbols represent young and filled symbols aged animals (Mean ± SEM).

Figure 2 – Analysis of histology. A: Identification of the primary auditory cortex. The pAC was identified by using the hippocampal fissure (HF: DG, dentate gyrus) as a reference structure. Three selected regions along the rostro-caudal axis are shown (from left to right, y coordinate relative to Bregma: -3.68; -3.005; -2.48 mm). The landmark was chosen according to the mouse brain reference atlas and centered under the microscope. By following a straight line, the camera section was moved to the cortex and the center of pAC was photographed. The magenta rectangle symbolizes the ROI which was used for the counting procedure. For the confirmation of the cortex position, see extended data (figure 2.1) and Tsukano et al., 2016. B: Example image with ROI for the counting of PV+ neurons. C: Example image with ROI for the counting of Nissl-stained neurons. Detailed image: Distinguishing between neurons and other cell types (arrow: neuron; asterix: non-neuronal cell type).

Figure 3 – Total number of neurons and PV+ immunoreactivity of the different groups. Circles depict B6 animals, squares display animals from the B6.CAST line. Open symbols represent young and filled symbols aged animals (Mean ± SEM). A: Mean total number of neurons. No significant difference could be revealed for the total number of neurons. B: Mean number of PV+

483 neurons. When compared to youngB6/B6.CAST, both agedB6 and agedB6.CAST show a
484 significant decrease in number of positive neurons ($p < 0.001$). C: Mean PV+ density. Young
485 animals show a significant higher density of PV+ neurons (youngB6/B6.CAST vs. agedB6: $p <$
486 .01; young vs. agedB6.CAST: $p = 0.001$).

487 Figure 4 – Distribution of PV+ neurons across layers and along the rostro-caudal axis. A:
488 Illustration of the relative laminar mapping of the cell positions within the single slices. The pia
489 was set to depth = 0 and the border to white matter was set to depth = 1. B: Population overview.
490 Relative density of PV+ neurons resolved by the rostro-caudal position of slices and cortical
491 depth of cell body is shown. Here, density was averaged over all slices from all animals to reveal
492 an age-independent overview about the general PV pattern in the primary auditory cortex.
493 Density was normalized to the maximum of the distribution. C: Cell density resolved by rostro-
494 caudal position of the slices (relative to bregma). Each bar depicts mean density for all slices
495 within the respective bin along the rostro-caudal axis. Left: young animals of both lines; middle:
496 agedB6 group; right: agedB6.CAST group. D: Laminar distribution of PV+ neurons in the three
497 groups (mean SEM). Positions are relative to the pia (see A). E: Relative density of PV+
498 neurons in the slices resolved by rostro-caudal position and cortical depth in the three groups.
499 Color-coded densities are normalized to the maximum mean density in the young group (left:
500 youngB6/B6.CAST, middle: agedB6, right: agedB6.CAST). Plots (B-E) were generated using
501 MATLAB (Version R2018b, Natick, Massachusetts: The MathWorks Inc.).

502 Fig. 2.1 - Confirmation of the position of auditory cortex in B6.cast mice. (A) A movable
503 electrode array was implanted, stereotactically positioned at 2.6 mm anterior to bregma. The path
504 of the probe was angled at 24° in order to follow the path indicated by the black line. Arrow
505 heads indicate the positions of the starting point after surgery and the last position that was

recorded from in the subject with furthest travel of the probe. Final positions varied from subject to subject. Recordings were obtained from an array of 8 tetrodes at each position in awake, unrestrained animals, typically yielding 20-30 units per position. The orange area depicts cortical fields labeled as 'auditory areas' according to the Allen mouse brain reference atlas (version 2012), which is based on tracing data. The thick yellow line at the top of the cortex indicates auditory areas in B6/C57 mice as determined by a study using physiological imaging (Tsukano et al. 2016). The red box is our window for counting PV+ cells, aligned by anatomical landmarks at 2.6 anterior to bregma. (B) Proportion of auditory and non-auditory units recorded at each position along the probe path. Each horizontal sequence of pie charts represents data from a single animal (n=6), the horizontal position of the pie center marks the position of the probe along the path. The grey area depicts the medial-lateral position of the window used for counting PV+ cells at 2.6 anterior to bregma. Each pie chart displays the proportion of non-auditory units (white), determined by a stimulus set containing both simple tone and complex naturalistic stimuli. Auditory units were classified as primary (blue) and non-primary (red) based on response latency (<20ms) to tone stimuli, responsiveness to repeated simple stimuli, and the shape of the frequency tuning curve. Data was collected in the context of another study, for further methodological details see Gothner et al., 2019.

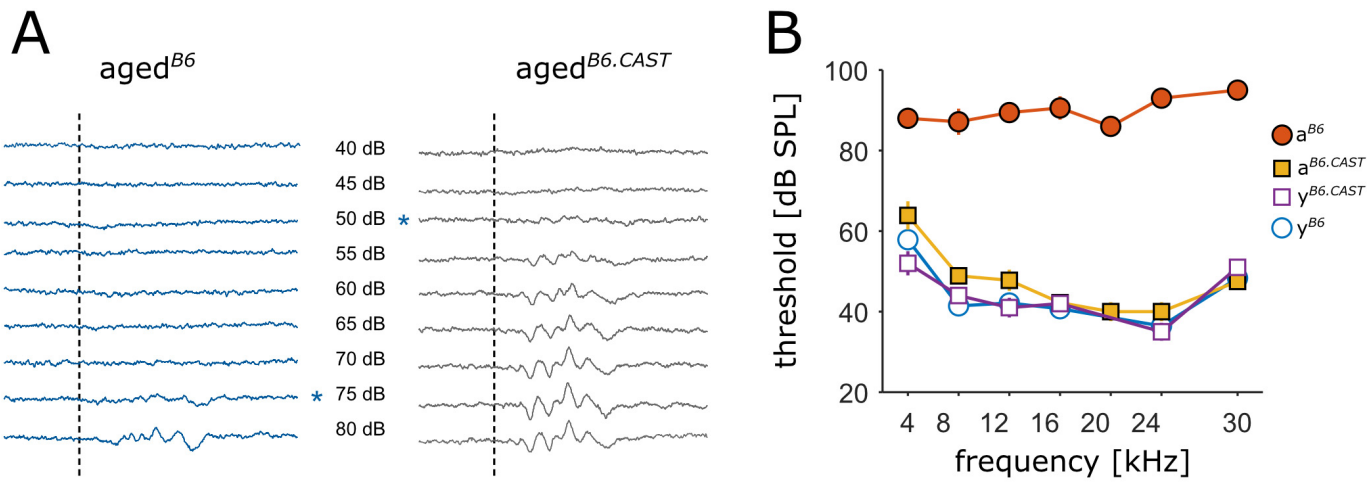

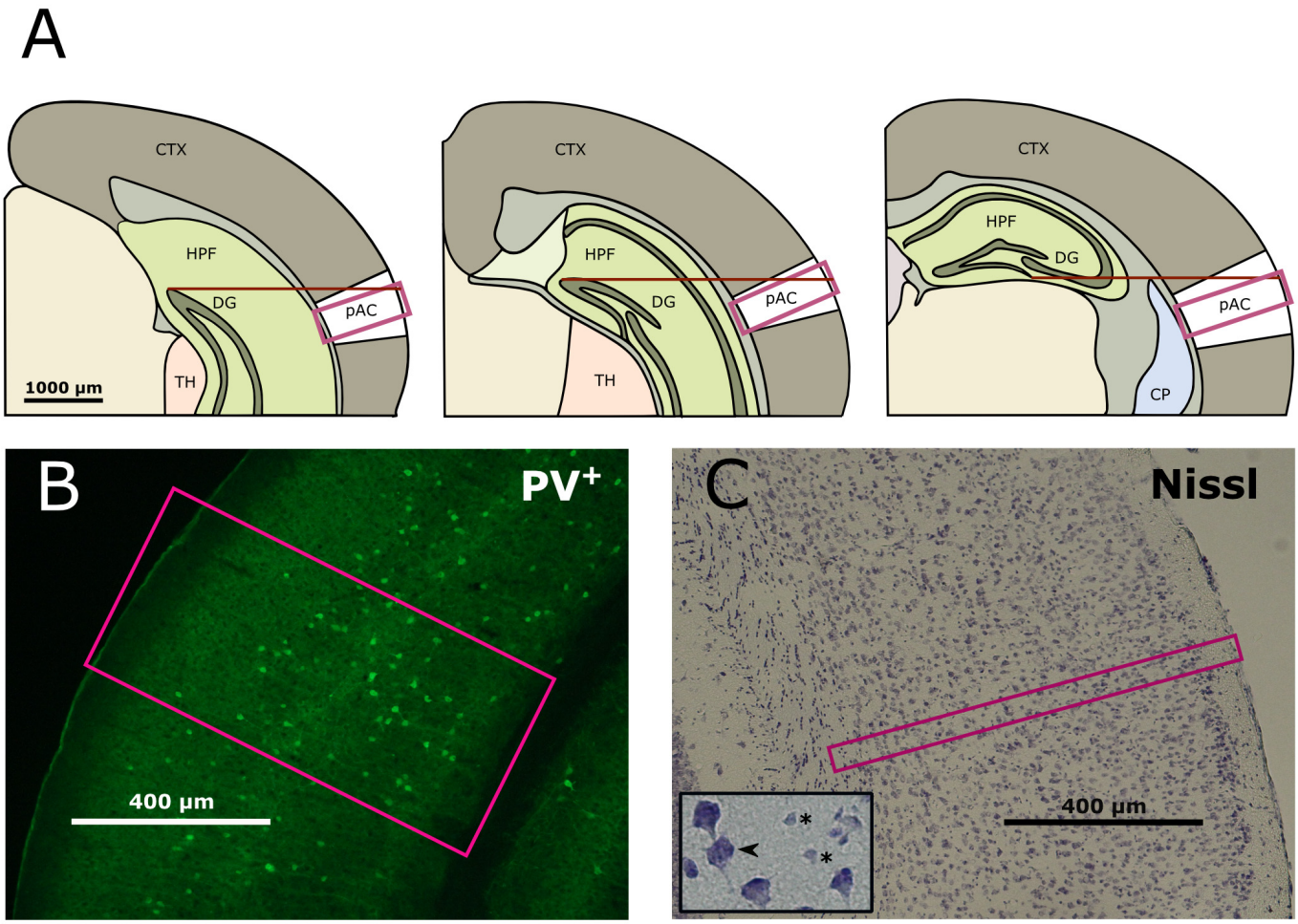

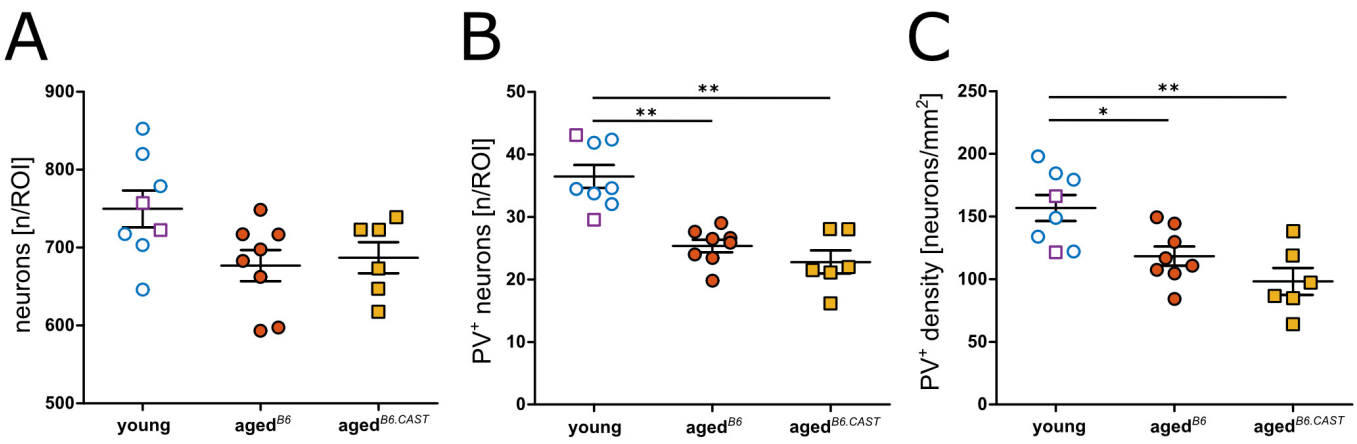

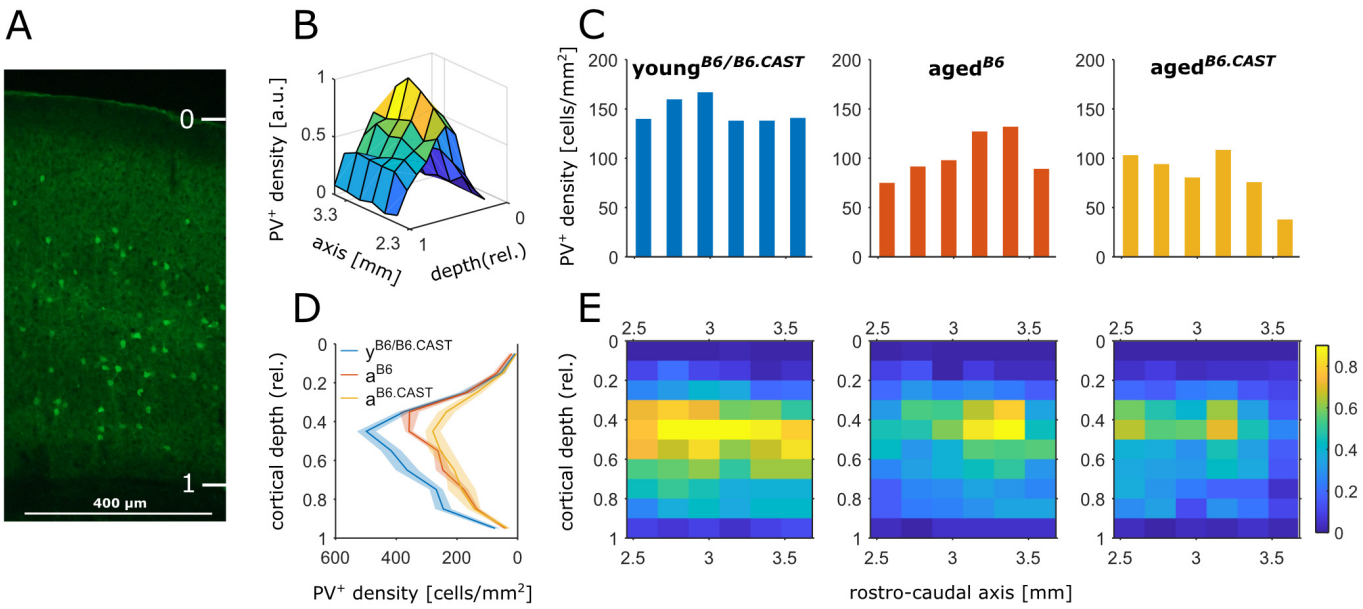

Table 1: Assignment of animals to the groups according to hearing status and age.

Group	age	histology	ABR	double	total
young^{B6}	10-12 w	6	6	1	11
young$^{B6.CAST}$	10-12 w	2	9	1	7
aged^{B6}	12-15 m	8	7	2	13
aged$^{B6.CAST}$	12-15 m	6	9	3	12
Sum:		22	28	7	43

Table 2: Statistics

Ref#	Data Structure	Parameters tested	Type of Test	Power (1-β err prob)	Figure
A	3 independent samples: young$^{B6/B6.CAST}$ (n = 8) aged^{B6} (n = 8) aged$^{B6.CAST}$ (n = 6)	Total number of neurons/ROI	ANOVA	0.3739166	3A
B	3 independent samples: young$^{B6/B6.CAST}$ (n = 8) aged^{B6} (n = 8) aged$^{B6.CAST}$ (n = 6)	Number of PV $^{+}$ interneurons/ROI	ANOVA	0.9993094	3B
C	3 independent samples: young$^{B6/B6.CAST}$ (n = 8) aged^{B6} (n = 8) aged$^{B6.CAST}$ (n = 6)	Density of PV $^{+}$ interneurons, number of PV^{+}/mm^{2}	ANOVA	0.8839026	3C